Scattering of Electromagnetic Radiation by a Large, Absorbing Sphere

Abstract: Details are provided for two subroutines with which one can compute the various characteristics of the electromagnetic radiation scattered by an absorbing, homogeneous sphere of any reasonable size. The necessary expressions for this purpose were first derived by Mie. The method of computations used is the so-called method of logarithmic derivative of one of the complex functions, introduced by Infeld. The main difference between the two subroutines is in the procedure used in computations of one of the functions. This function is computed by an upward recurrence procedure in one subroutine and by a downward recurrence procedure in the other. Sufficient results for demonstrating the reliability of these programs are presented and discussed for a sphere of 10μm radius illuminated by an unpolarized radiation of 0.4μm wavelength.

1. Introduction

The passage of electromagnetic radiation through a medium is generally accompanied by the removal of a fraction of the energy from the incident beam. This fraction may be partly absorbed within the medium, and may become partly scattered, i.e., reappear in the same direction as well as in other directions. The characteristics of the scattered radiation are determined by the wavelength λ of the incident radiation, the complex refractive index $(m = n_1 - in_2)$ of the medium, and the size as well as the shape of the discrete particles in the medium. Because of this, measurements and proper interpretation of the characteristics of the scattered radiation offer a very good opportunity for obtaining information about the state of the medium. Hence, numerical determination of the characteristics of the scattered radiation for a given model is of prime importance in several diversified fields such as planetary and atmospheric optics; astrophysics; laser. radar, and searchlight applications; and physical chemistry. To this end, the first step is the evaluation of the characteristics of the radiation scattered by a single particle.

The numerical evaluation of the parameters of the radiation scattered by a particle very small compared to λ is very simple and straightforward. The expressions for the radiation scattered by a sphere whose radius (r) is comparable to, or greater than, λ were first derived by Mie. The expressions for Mie scattering involve series whose terms contain Bessel functions of half-integral order (spherical Bessel functions) with complex argument,

and first and second derivatives of the Legendre polynomials. Furthermore, the number of terms required for evaluating the series is of the order of the size parameter x (i.e., $2\pi r/\lambda$). Hence, the reliable Mie scattering computations for large spheres can be described as difficult, tedious, and time consuming.

The derivations of the Mie expressions as well as a catalog of its available numerical solutions in some specific cases can be found in the treatise, "Light Scattering by Small Particles," by Van de Hulst.3 Prior to this publication, numerical evaluation of the Mie expressions was confined to small values of $x(\sim 10)$ for absorbing $(n_2 > 0)$ spheres. For nonabsorbing spheres $(n_2 = 0)$, the most outstanding work is that of Gumprecht and Sliepcevich, 4,5 who carried their calculations to x = 400. As has been pointed out by Van de Hulst,3 the work of these authors cannot be considered to be complete since the laws of geometric and physical optics can be applied to the transfer problem in a water sphere with some reasonable confidence only if x is of the order of 2000. Even for x this high, Van de Hulst points out some limitations of such a ray optics treatment and a need for checking such results against those obtained using the exact solution.2 Furthermore, the number of directions for which the radiation parameters are given by these authors⁵ is too small to give any insight into the fine structure of the radiation field. Besides, many fields of application demand extensive numerical data for values of refractive indices other than those used by these authors.⁵

Since the publication of Van de Hulst's book, several authors⁶⁻¹⁵ (references are by no means exhaustive) have

The author is located at the IBM Scientific Center, 2670 Hanover Street, Palo Alto, California

published useful results for absorbing spheres of moderate size ($x \sim 50$). For nonabsorbing spheres, the trend is to obtain a much more detailed picture of the field of the scattered radiation than was available before¹⁶⁻¹⁸ and to compute the average characteristics of the radiation scattered by a unit volume containing an arbitrary size distribution of small spherical particles (x < 200).¹⁹⁻²² Very recently, Fahlen and Bryant²³ have reported results of some of their computations for $x \sim 3000$ but for only one direction of scattering ($\theta = 180^{\circ}$).

This slowness of progress in obtaining the radiation field for large spheres may be attributed partly to the limited requirements of previous workers. However, since Mie computations involve evaluation of series whose terms differ by several orders of magnitude with increase of n and change their signs in rather uneven manner, it is essential to carry out basic arithmetic in double precision if x is large. The other factor is the large storage requirements. Computations of the radiation scattered in 37 different directions [0°(5°)180°] by a sphere having size parameter x = 1000 with straightforward programming procedure can require use of more than 100,000 doubleprecision words of storage, a requirement too large to be fulfilled by the main storage area of any modern computer. Hence, one is required to use magnetic tapes or disks.

The main difficulty in evaluation of the characteristics of the radiation scattered by a large absorbing sphere is the very rapid propagation of the errors when the function $A_n(mx)$ (Sec. 2.1) is computed using an upward recurrence relationship (Sec. 2.2). A recurrence relationship provides a very powerful computing tool, especially in automatic work. However, since generation is carried out perforce with rounded values, the errors may or may not grow relative to the size of the wanted function. If the errors do grow, the recurrence scheme is said to be unstable. When the upward recurrence scheme [i.e., starting with the value of $A_0(mx)$, one computes successively higher values of $A_n(mx)$ by making use of a recurrence formula] is unstable, in general the downward recurrence scheme is found to be very stable.24 It is not necessary to know the initial value for starting the downward recurrence scheme; one can make use of the ratio method first described by Miller.25 Reference may also be made of an independent later work in this direction by Corbató and Uretsky,26 who have applied the downward recurrence procedure for generation of spherical Bessel functions on digital computers. Kattawar and Plass¹² seem to be the first to use this downward recurrence procedure in Mie scattering calculations.

After a careful analysis of the various problems of the Mie scattering computations described above, two computer subroutine programs (FORTRAN IV G language) were developed recently by the author.²⁷ They were then used to study the characteristics of the radiation scattered by large ($x \sim 800$), nonabsorbing spheres.²⁸ The purpose of this paper is to describe some major features of these subroutine programs and to present some of the results for a large, absorbing sphere.

2. A second look at the Mie expressions

From the expressions for the radiation scattered by a sphere given in the Appendix, it can be seen that the computational problem reduces to that of evaluating the following four quantities: The complex quantities a_n and b_n (Eqs. 32 and 33) which are functions of the size parameter (x) and refractive index $(m = n_1 - in_2)$ of the material of the sphere, and the functions π_n and τ_n (Eqs. 41 and 42) which are functions of the scattering angle (θ) .

• 2.1 a_n and b_n :

The expressions for the functions a_n and b_n [Eqs. (32) and (33)] for complex values of the parameter m contain the spherical Bessel functions $j_n(mx)$ which in turn require hyperbolic sine and hyperbolic cosine functions $\sinh (n_2x)$ and $\cosh (n_2x)$. Since all computers deal only with finite numbers, the evaluation of the expressions in the present form can result in an overflow. For IBM System/360 computers, this overflow occurs when $n_2x \sim 170$.

This overflow can be avoided by dividing both numerator and denominator of the expression for a_n as well as that of b_n by $j_n(mx)$ as all the terms contain $j_n(mx)$ or $j_{n-1}(mx)$. Infeld, ³³ who seems to have been the first to recognize this, introduced the so-called logarithmic derivative of $\Psi_n(mx)$ and $\xi_n(x)$ functions given by Eqs. (34) and (35), respectively. Some of the properties of these logarithmic derivative functions have been discussed by Aden. ³⁴ The function

$$\frac{d[\log \Psi_n(mx)]}{d(mx)} = \frac{\Psi'_n(mx)}{\Psi_n(mx)} \tag{1}$$

is denoted as $\sigma_n(mx)$, $A_n(mx)$, or as $D_n(mx)$ function in Refs. 34, 9, and 12, respectively. By use of this ratio, which we will call $A_n(mx)$, the expression for $a_n(x, m)$ can be written as follows:

 $a_n(x, m)$

$$= \frac{\left\{\frac{A_n(mx)}{m} + \frac{n}{x}\right\} \operatorname{Re}\left[\xi_n(x)\right] - \operatorname{Re}\left[\xi_{n-1}(x)\right]}{\left\{\frac{A_n(mx)}{m} + \frac{n}{x}\right\} \xi_n(x) - \xi_{n-1}(x)}, \quad (2)$$

and

$$b_n(x, m)$$

$$= \frac{\left\{ m A_n(mx) + \frac{n}{x} \right\} \operatorname{Re} \left[\xi_n(x) \right] - \operatorname{Re} \left[\xi_{n-1}(x) \right]}{\left\{ m A_n(mx) + \frac{n}{x} \right\} \xi_n(x) - \xi_{n-1}(x)}.$$
 (3)

After making use of the recurrence relationship given by Eq. (38), it can be shown that the functions $A_n(mx)$ and $A_{n-1}(mx)$ are related as follows:

$$A_{n}(mx) = -\frac{n}{mx} + \frac{j_{n-1}(mx)}{j_{n}(mx)}$$

$$= -\frac{n}{mx} + \frac{1}{\frac{n}{mx} - A_{n-1}(mx)}.$$
(4)

The following initial value for setting up this recurrence can be obtained after making use of Eqs. (39) and (40):

$$A_0(mx) = \frac{j_{-1}(mx)}{j_0(mx)} = \cot(mx).$$
 (5)

The values of the function $\xi_n(x)$ can be computed after making use of the following recurrence relationship based on Eqs. (38) to (40).

$$\xi_n(x) = \frac{2n-1}{x} \, \xi_{n-1}(x) \, - \, \xi_{n-2}(x), \tag{6}$$

with

$$\xi_{-1}(x) = \cos x - i \sin x,\tag{7}$$

and

$$\xi_0(x) = \sin x + i \cos x. \tag{8}$$

At first sight, modified expressions of $a_n(x, m)$ and $b_n(x, m)$ as given by Kattawar and Plass¹² appear to be different from those given by Deirmendjian and Clasen.⁹ This is not really the case and one can check their equivalence by making use of Table 1.

• 2.2 A_n and ξ_n

The initial value for setting up the recurrence procedure for computations of $A_n(mx)$ is given by Eq. (5). With $m = n_1 - in_2$, it can be written in either of the following forms:

$$A_0(mx) = \frac{\sin(2n_1x) + i\sinh(2n_2x)}{\cosh(2n_2x) - \cos(2n_1x)},$$
 (9)

or

 $A_0(mx)$

$$= \frac{\sin (n_1 x) \cos (n_1 x) + i \sinh (n_2 x) \cosh (n_2 x)}{\sin^2 (n_1 x) + \sinh^2 (n_2 x)}.$$
 (10)

If $n_2x = 0$ and n_1x is an integer multiple of π , either of these forms will give rise to a division by zero, and hence a possible termination of the program, or wrong results. (This problem does not arise if the downward recurrence procedure is used.) This is not a hypothetical case, as several situations can be visualized where $2n_1r/\lambda$ can be an integer. Because of the generation of the roundoff errors in a particular way, the expression for $A_0(mx)$

Table 1 Notations as used by Deirmendjian and Clasen⁹ and by Kattawar and Plass, 12

Deirmendjian and Clasen	Kattawar and Plass
Re $[W_n(x)]$	$\Psi_n(x)$
$W_n(x)$	$\xi_n(x)$
$A_n(mx)$	$D_n(mx)$
$\frac{\operatorname{Re}\left[W_{n-1}(x)\right]}{\operatorname{Re}\left[W_{n}(x)\right]} - \frac{n}{x}$	$D_n(x)$
$\frac{W_{n-1}(x)}{W_n(x)}-\frac{n}{x}$	$G_n(x)$

given by Eq. (10) was found to be more suitable for computational purposes. However, it will be necessary to apply due caution if $2n_1r/\lambda$ is very close to an integer, since roundoff errors are generated differently in different computers.

If $n_2 \neq 0$, a straightforward evaluation of $A_0(mx)$ will again run into trouble if $n_2x \sim 90$ or more. Since for these large values of n_2x , sinh $(n_2x) \sim \cosh(n_2x) \sim \frac{1}{2}e^{(n_2x)}$, we may make use of the following approximation:

$$A_0(mx) = 0.0 + 1.0 i. (11)$$

A use of this approximation immediately leads to the question of propagation of errors, as the successive values of $A_n(mx)$ are computed by upward recurrence [Eq. (4)]. As mentioned earlier (Sec. 1), Kattawar and Plass¹² have already pointed out that a numerical instability develops in this case. For setting up the downward recurrence procedure, they have suggested the use of 0.0 + 0.0i as the initial value of $A_N(mx)$ for some value of N > |mx|. Since the computational error decreases very rapidly at each step of downward recurrence in this particular case, the calculations are insensitive to the assumed starting value and converge very rapidly to the correct value. The following criterion for selecting the value of N at which the downward recurrence should be started was arrived at after trial and error:

$$N = 1.1(n_1^2 + n_2^2)^{\frac{1}{2}}x + 1. {(12)}$$

The real part of the function $A_n(mx)$ for m=1.342-1.0i and $x=50.0\pi$ as obtained after using the upward recurrence (thin solid curve) and downward recurrence (broken curve) procedures, is plotted in Fig. 1 as a function of n. It can be seen that a numerical instability develops in the upward recurrence scheme when n=111. Between 112 and 125, large oscillations develop. The amplitude of these oscillations decreases when n is about 130. For n=136 and higher, a stabilization occurs, but the real part of $A_n(mx)$ achieves a value which is completely different from the correct value given by the broken curve.

The ultimate effect of this instability is to increase the values of the efficiency factor Q_s [Eq. (44)]. Eventually, Q_s becomes greater than Q_s leading to negative values for Q_a [Eq. (45)]. An example of this is provided in Table 2, where the values of Q_a as obtained using the upward recurrence procedure, and as obtained using the downward recurrence procedure for computations of $A_n(mx)$, are tabulated for several values of n_2 . The assumed values of n_1 and x are 1.342 and 50.0 π , respectively. The values of Q_a as obtained using two different computational procedures agree to four significant figures for n_2 up to 0.2. For $n_2 = 0.3$, a difference of one unit is noticeable in the fourth significant place. Thereafter, the difference increases very rapidly, and for $n_2 \ge 0.5$, the use of upward recurrence procedure results in erroneous negative values of Q_a .

The computations of the function $\xi_n(x)$, which always has a real argument, are straightforward. The problem of the propagation of error is not serious if all the basic arithmetic is done in double precision.

• 2.3 π_n and τ_n

The phase functions $\pi_n(\mu)$ and $\tau_n(\mu)$ given by Eqs. (41) and (42) can be computed after making use of the following recurrence relationship based on the properties of the Legendre polynomials and their derivatives:

$$\pi_n(\mu) = \frac{2n-1}{n-1} \mu \pi_{n-1}(\mu) - \frac{n}{n-1} \pi_{n-2}(\mu), \qquad (13)$$

Figure 1 Variation of the real part of the complex function $A_n(mx)$ as a function of n. Broken curve represents values obtained by using downward recurrence procedure. Thin solid curve represents values obtained using upward recurrence procedure. m=1.342-1.0 i, $x=50.0\pi$.

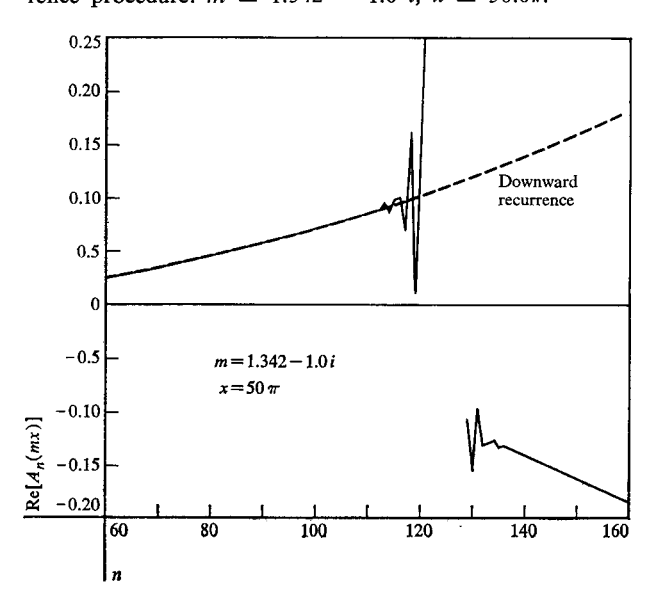


Table 2 The values of the efficiency factor for absorption Q_a as a function of n_2 : $m=1.342-n_2i$, $r=10.0\mu$, $\lambda=0.4\mu$, $x=50.0\pi$.

n_2	Column 2	Column 3
0.0	0.0000	0.0000
0.0001	0.0535	0.0535
0.001	0.4149	0.4149
0.01	0.9649	0.9649
0.1	0.9653	0.9653
0.2	0.9542	0.9542
0.3	0.9389	0.9390
0.4	0.4913	0.9211
0.5	-0.4925	0.9016
0.6	-0.5265	0.8808
0.7	-1.1592	0.8592
0.8	-2.3079	0.8369
0.9	-1.4379	0.8141
1.0	-1.3789	0.7910

Column 2: Values of Q_0 as obtained after computing the function $A_n(mx)$ using an unward recurrence procedure

using an upward recurrence procedure.

Column 3: Values of Q_a as obtained after computing the function $A_n(mx)$ using a downward recurrence procedure.

and

$$\tau_n(\mu) = \mu[\pi_n(\mu) - \pi_{n-2}(\mu)] - (2n-1)(1-\mu^2)\pi_{n-1}(\mu) + \tau_{n-2}(\mu), \quad (14)$$

where

$$\pi_{0}(\mu) = 0,
\pi_{1}(\mu) = 1,
\tau_{0}(\mu) = 0,
\tau_{1}(\mu) = \mu$$
(15)

Computations of the values $\pi_{3000}(\mu)$ and $\tau_{3000}(\mu)$ starting with those of $\pi_0(\mu)$, etc., given by Eq. (15) results in a loss of six to seven significant figures. Hence, it is again necessary to carry out basic arithmetic in double precision.

The values of $\pi_n(1)$ and $\tau_n(1)$ obtained after making use of Eqs. (13), (14), and (15), can be checked against those obtained from the following very simple expressions for the same:³

$$\pi_n(1) = \tau_n(1) = \frac{1}{2}n(n+1). \tag{16}$$

For $\theta = 90^{\circ}$, i.e., $\mu = 0$, it can be shown that

$$\pi_{n}(0) = 0 \quad \text{(if } n \text{ is even)}$$
and
$$\pi_{n}(0) = \frac{2(-1)^{(n-1)/2} \Gamma(\frac{n}{2} + 1)}{\Gamma(\frac{n}{2} + \frac{1}{2}) \Gamma(1/2)} \quad \text{(if } n \text{ is odd)}$$
(17)

The values of gamma functions for large values of n can be found in one of the tables in the series of mathematical tables published by the U. S. National Bureau of Standards.³⁵

If the values of $\pi_n(\mu)$ and $\tau_n(\mu)$ for $\mu > 0$ have already been computed, it is not necessary to compute those of $\pi_n(-\mu)$ and $\tau_n(-\mu)$, as has been done by some investigators (e.g., Ref. 4). Instead, one can make use of the following relationships:

$$\pi_n(-\mu) = (-1)^{n-1}\pi_n(\mu) \tag{18}$$

and

$$\tau_n(-\mu) = (-1)^n \tau_n(\mu). \tag{19}$$

These relationships can be derived easily by making use of the following well-known properties of the Legendre polynomials:

$$P_n(-\mu) = (-1)^n P_n(\mu), \qquad (\mu \ge 0)$$
 (20)

and

$$P'_n(-\mu) = (-1)^{n-1}P'_n(\mu), \qquad (\mu \ge 0), \tag{21}$$

where P'_n represents the derivative of P_n with respect to μ . However, it appears that the above mentioned properties have gone unnoticed in this particular field. Van de Hulst³ has not given them explicitly, even though he does make use of these relationships for $\mu = -1$ at several places. The later investigators (e.g., Refs. 6, 9, 12, 13, and 16) do not refer to them either. The advantages of making use of these relationships should be more evident after studying the published data of various authors and after recognizing the ease of obtaining data for the supplementary angles.²⁷

3. Results of computation

• 3.1 Some characteristics of the subroutine programs After making use of the formulas and the procedure outlined in Sec. 2 above, two double-precision subroutines were written in FORTRAN IV G language. In one of these subroutines, all the basic functions [i.e., $A_n(mx)$, $\xi_n(x)$, $a_n(mx)$, $b_n(mx)$, $\pi_n(\mu)$ and $\tau_n(\mu)$] are computed using the upward recurrence procedure. In order to cut down on the exorbitant and unnecessary storage demand, the series for $S_1(x, m, \theta)$, $S_2(x, m, \theta)$, $Q_s(x, m)$, $Q_s(x, m)$, and $\cos \theta$. $Q_s(x, m)$ given by Eqs. (28), (29), (43), (44), and (46), respectively are updated after computation of the basic functions of a current order, and the storage space for the basic functions is re-used unless their values are required at a later stage. The computations are terminated when the following criterion is satisfied:

$$|a_n(x, m)|^2 + |b_n(x, m)|^2 < 1.0 \times 10^{-14}.$$
 (22)

Table 3 Average time (t in seconds) which the first subroutine takes to return values of four elements of the transformation matrix for 182 values of θ as well as values of Q_{θ} , Q_{θ} , and $\cos \theta \cdot Q_{\theta}$ for various values of size parameter x. Computing facility used: IBM System/360 Model 50, FORTRAN IV G compiler, Level 1, Mod. 2.

x	t in sec	
0.1	0.7	
1.0	1.1	
10.0	3.7	
100.0	22.	
1000.0	194.	
5000.0	945.	

The sparing use of storage space and the use of relationships given by Eqs. (18) and (19) resulted in obtaining the values of the elements of the transformation matrix in as many as 200 different directions with a nominal storage requirement of 11,962 bytes (FORTRAN IV G, Level 1, Mod 2). It should be noted that this subroutine was used to obtain reliable numerical results for a nonabsorbing sphere with size parameter up to 5000.

In the other subroutine where one of the basic functions, $A_n(mx)$ is computed by downward recurrence, the storage requirement is rather high as all the values of $A_n(mx)$ have to be stored for later use. It is 123,868 bytes if recurrence is to be started at an order as high as 7000 and output is desired in 200 different directions. Furthermore, even for this much core storage, the maximum value of x for which output can be obtained is determined by values of n_1 and n_2 as can be seen from Eq. (12).

Average time (t in seconds) which the first subroutine takes to return values of four elements of the transformation matrix for 182 values of θ , as well as values of Q_* , Q_* , and $\cos \theta$. Q_* is given in Table 3 as a function of the size parameter x. Because of the use of the downward recurrence procedure in the computations of $A_n(mx)$, the average time for the second subroutine depends upon the values of n_1 , n_2 , and x. For $1.0 < (n_1^2 + n_2^2)^{\frac{1}{2}} < 1.5$, this subroutine requires, on average, about 10 to 20% more time than the first one.

Because of the nature of the problem, it is not possible to make a positive statement about the reliability of a given value. However, after comparison of the values obtained using these subroutines with some published and unpublished results $^{(3,4,6-10)}$ and, after detailed investigation of the error propagation problem, it is felt that the first six significant figures should be generally reliable if the sphere is not very large. For a very large sphere ($x \sim 3000$ and higher), only the first four or five significant figures should be considered reliable.

Further confidence in the numerical results can be gained by comparing some values given by these subroutines with those which can be obtained from some simple formulas applicable in extreme cases. One of such formulas is given on pages 264 and 265 of Ref. 3. Accordingly, for a large sphere made of material with refractive index m = 1.342 - 0.0i, Q_* , the efficiency factor for scattering, can be calculated from the following "best" formula:

$$Q_{\bullet} = 2.0 - 7.680x^{-1} \sin(0.684x) + 1.84(x)^{-\frac{3}{4}} + \text{"ripple"}.$$
 (23)

For $x = 50.0\pi$ and 500.0π , the values of Q_{\bullet} obtained from this formula are 2.0345 + "ripple" and, 2.0136 + "ripple", respectively, which compare well with the respective values of 2.0305 and 2.0129 given by the subroutines.

The other such formula is for the intensity of the radiation backscattered by a sphere made of highly absorbing material. In the absence of any contribution by the rays travelling through the sphere, the intensity of the backscattered radiation $(I_{\theta-180}^{\circ})$ can be obtained from the following formula, based on Fresnel's law of reflection:

$$I_{\theta=180} = \frac{x^2}{4} \left[\frac{(n_1 - 1)^2 + n_2^2}{(n_1 + 1)^2 + n_2^2} \right]$$
 (24)

Using this equation, we have $I_{\theta=180^{\circ}}=1.06246\times 10^3$ and 1.42526×10^4 for $x=50.0\pi$, m=1.342-1.0i, and, $x=500.0\pi$, m=1.342-0.1i, respectively. The corresponding values as obtained using the subroutines are 1.06248×10^3 and 1.42526×10^4 , respectively. These comparisons aptly support the reliability claims described earlier in this section.

• 3.2 Scattering by an absorbing sphere

In a recent paper, 28 the author has demonstrated the usefulness of these subroutine programs in carrying out exhaustive studies of the characteristics of the radiation scattered by large, nonabsorbing spheres. In this section, we propose to present and to discuss the results for an absorbing sphere with $r=10.0\mu\mathrm{m}$ and illuminated by a parallel beam of unpolarized, monochromatic radiation having $\lambda=0.4\mu\mathrm{m}$. The sphere is assumed to be made of a material whose refractive index with respect to its surrounding is given by $m=1.342-n_2i$. The value of n_2 is varied from 10^{-5} to 1.0. This particular case is selected to study the effects of varying absorption on some prominent optical features such as the rainbow and glory.

Before going into the details of the characteristics of the scattered radiation field, we shall look into the effect of varying absorption on some of the specific and integrated optical properties of the sphere. In Fig. 2, the

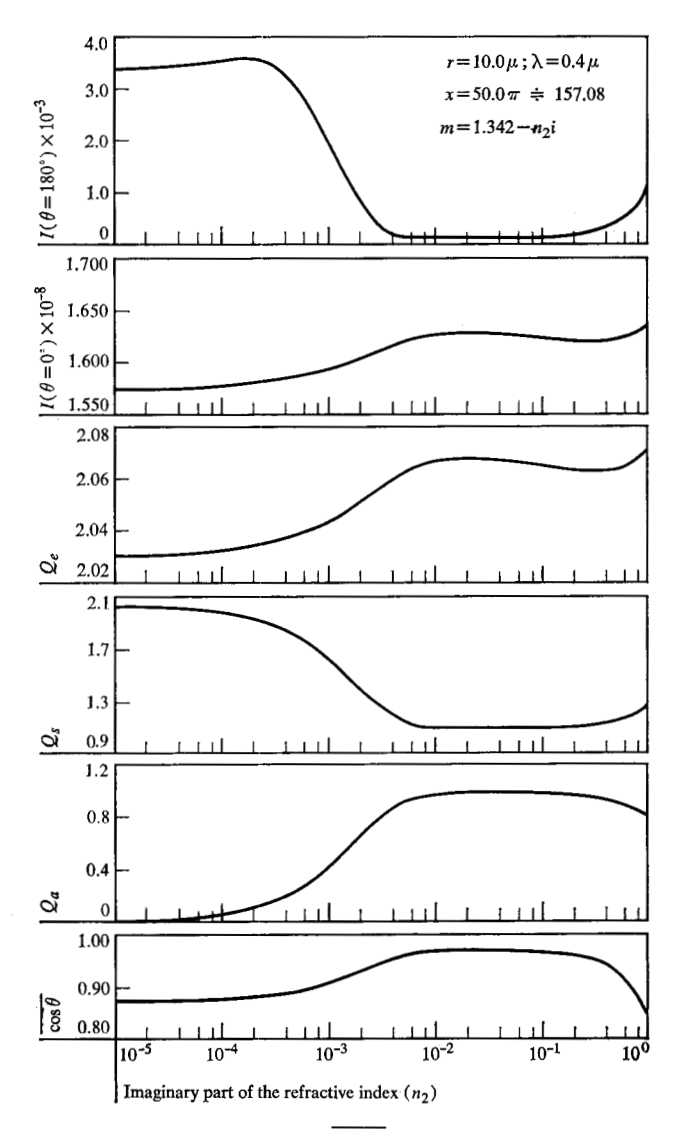


Figure 2 Variation of the $\overline{\cos \theta}$, Q_a , Q_s , Q_e , $I_{(\theta=0^\circ)}$ and $I_{(\theta=180^\circ)}$ as a function of the imaginary part of the refractive index.

second curve from the bottom (marked Q_a) represents the variation of the efficiency factor for absorption (Eq. 45) as a function of n_2 . For $n_2 \sim 10^{-5}$, the sphere absorbs a very minute fraction of the radiation incident upon it; in fact, for $n_2 = 1.0 \times 10^{-5}$, $Q_a = 0.0055$. As the imaginary part of the refractive index (n_2) is increased from 10^{-4} to 10^{-2} , Q_a increases rather rapidly from 0.054 to 0.965. For a further order-of-magnitude increase in the value of n_2 , Q_a shows very little change. For still larger values of $n_2(>0.1)$, a significant decrease in the absorbing power of the sphere is due to an increase in reflecting properties of the material of the sphere (Fresnel's law). The efficiency factor for scattering $(Q_a$, Eq. 44) decreases with increase of absorption, attains a constant value when Q_a is independent of n_2 , and increases with n_2 when the reflecting

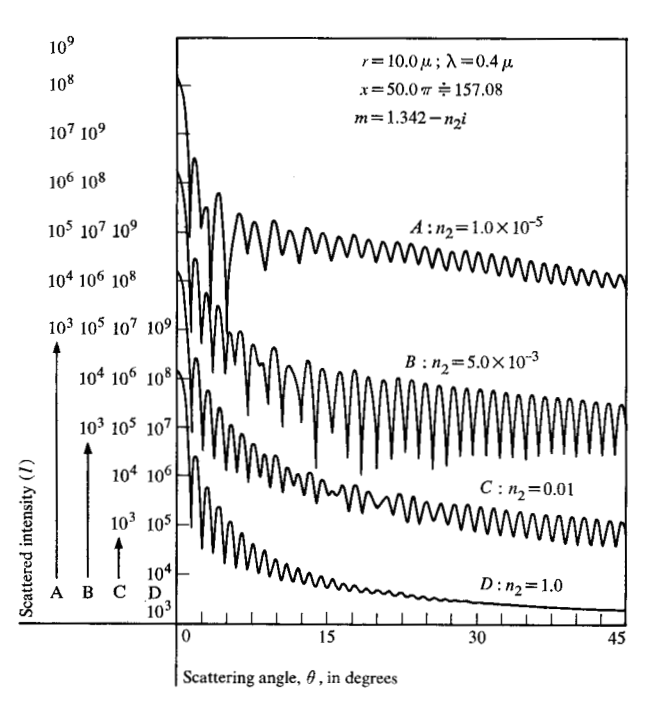


Figure 3 Variation of the scattered intensity as a function of the scattering angle; $0^{\circ} \le \theta \le 45^{\circ}$.

power of the sphere increases. The middle curve, marked Q_{\bullet} , shows the variations in the efficiency factor for extinction (Eq. 43) as a function of n_2 . As mentioned in the Appendix, Q_{\bullet} is the sum of Q_a and Q_{\bullet} .

The intensity of the radiation scattered in the forward direction (broken curve in Fig. 2) shows a significant increase in the region $10^{-4} < n_2 < 10^{-2}$ where the absorption plays an increasingly important role. The radiation in this direction is a resultant of an interaction between the radiations diffracted, transmitted and reflected by the sphere (anomalous diffraction, Sec. 13.41 of Ref. 3). Even though the diffracted component plays the most important role, the contribution due to the other two is evident. Furthermore, since the reflected component undergoes very little change, an increase in $I_{\theta=0}$ ° as a function of n_2 in the range 10^{-4} to 10^{-2} can be explained by postulating a destructive interference between the radiations diffracted and transmitted by the sphere.

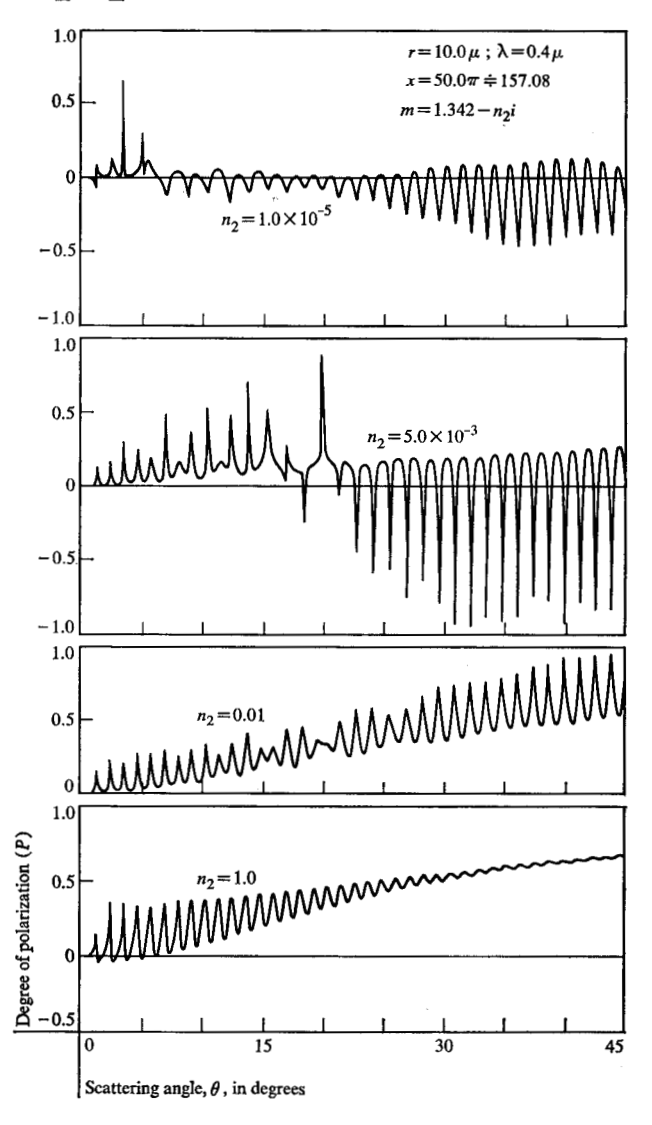
The variations of $I_{\theta-180}$ ° as a function of n_2 (top curve) can also be similarly explained. A strong decrease in the magnitude of the backscattered intensity, in the region where absorption starts playing an increasingly more important role, is due to the strong attenuation of the radiation which returns from the sphere after suffering one internal reflection (p = 2 in Fig. 7).

The lowermost curve in Fig. 2 (marked $\cos \theta$) represents the variations of the so-called asymmetry factor (Eq. 46) as a function of n_2 . This factor gives a gross indication about the way in which the scattered energy is distributed

around a plane at right angle to the incident radiation, e.g., for isotropic and Rayleigh scattering, this quantity vanishes. The variations in $\cos \theta$ as a function of n_2 are better understood after examining the details of the characteristics of the scattered radiation field.

The variations of the intensity and degree of polarization of the radiation scattered by a 10.0μ sphere are shown in Figs. 3 and 4 for the angular region 0° -45°. Similar results for the angular regions 45° -90°, 90° -135°, and 135° -180° are shown in Figs. 5, 6, and 9-12. As mentioned earlier, the sphere is assumed to be illuminated by a plane parallel beam of unpolarized radiation with $\lambda = 0.4\mu$. The computations were carried out for the 1801 values of θ given by $\theta = 0.0^{\circ}(0.1^{\circ})180.0^{\circ}$. The results presented in these diagrams were plotted using an IBM 1627 plotter

Figure 4 Variation of the degree of polarization of the scattered radiation as a function of the scattering angle; $0^{\circ} \le \theta \le 45^{\circ}$.



and the successive points were joined by straight lines. Because of the finite number of angular positions at which the computations were made, the actual maxima and minima can be much more pronounced than shown, especially if they appear very pointed in these diagrams.

After a careful study of the detailed output for about 20 values of n_2 in the range 10^{-5} to 1.0, output for four different values of $n_0(1.0 \times 10^{-5}, 5.0 \times 10^{-3}, 0.01)$ and 1.0) was selected to study the effect of varying absorption on the characteristics of the scattered radiation. In the region 0°-15°, the pronounced contribution due to diffraction is very evident. Because of this, the intensity (Fig. 3) and degree of polarization (Fig. 4) of the scattered radiation show only minor changes as the imaginary part of the refractive index is increased by five orders-ofmagnitude. With increase in θ , the contribution due to diffracted radiation decreases rapidly, and the contribution due to interaction between the radiations reflected and transmitted by the sphere plays an important role. For $\theta > 45^{\circ}$, and $n_2 = 1.0$, the reflected radiation is a prime contributor as can be seen from very strong damping of the oscillations.

In the angular region $45^{\circ}-90^{\circ}$, the interesting feature is the maximum in the degree of polarization curve (Fig. 6) at the pseudo-Brewster angle $[180^{\circ} - 2 \tan^{-1} |m|]$ as predicted by ray optics. As expected, the position of this maximum shifts towards the forward direction with increase of n_2 .

Some of the features of the scattered intensity field in the angular region 90°-180° are predicted by ray optics. If the radius of the sphere is large compared to the wavelength of the incident radiation, the incident beam can be broken up into several narrow sub-beams or rays whose width is much greater than λ but small compared to r. Let us consider one such ray making an angle τ with the surface (Fig. 7). $\tau = 90^{\circ}$ for the central ray and $\tau = 0^{\circ}$ for the edge ray. The incident ray is partly reflected along the direction marked 0, and is partly refracted along the direction making an angle τ' with the surface. The relation between τ , τ' and refractive index m is given by Snell's law. The refracted ray suffers several internal reflections and at each reflection, a part of the energy leaves in the directions marked p = 1, 2, 3, etc.

In Fig. 8, we have shown the variations in scattering angle θ at which the ray emerges after undergoing one (p=2) or two (p=3) internal reflections. For p=2, the central ray bounces back, and emerges in a direction marking an angle of 180° with that of the incident radiation. θ decreases with τ , passes through a minimum value of 139.2° at $\tau=31.1^{\circ}$, and then increases for further decrease in τ . The edge ray $(\tau=0^{\circ})$ emerges at $\theta=167.3^{\circ}$. The position of the minimum deviation is generally referred to as that of the primary rainbow.

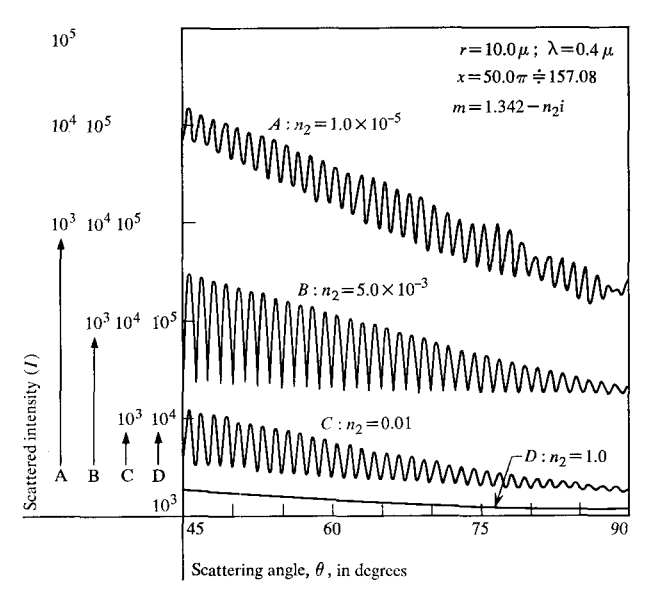
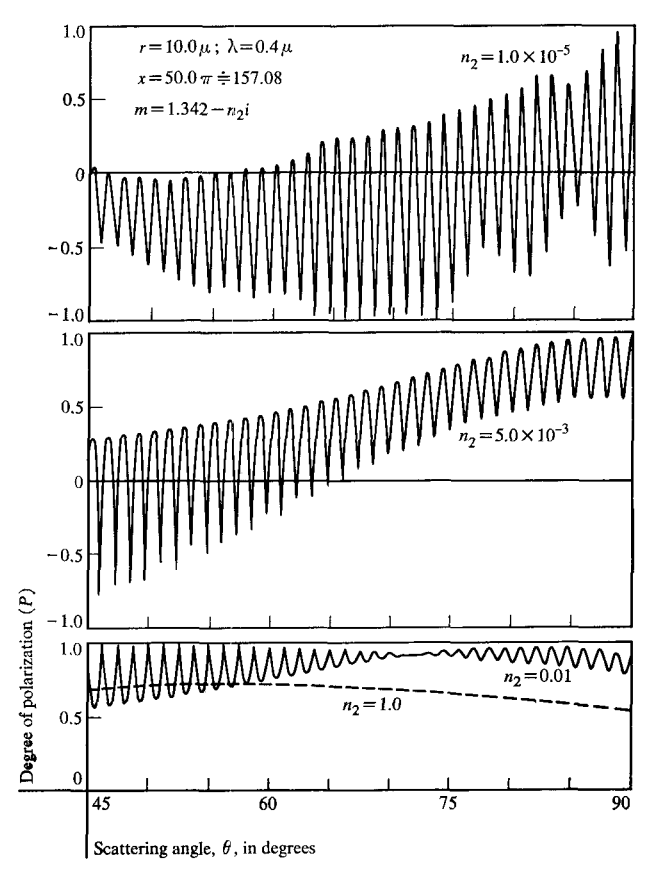


Figure 5 Variation of the scattered intensity as a function of the scattering angle; $45^{\circ} \le \theta \le 90^{\circ}$.

Figure 6 Variation of the degree of polarization of the scattered radiation as a function of the scattering angle; $45^{\circ} \leq \theta \leq 90^{\circ}$.



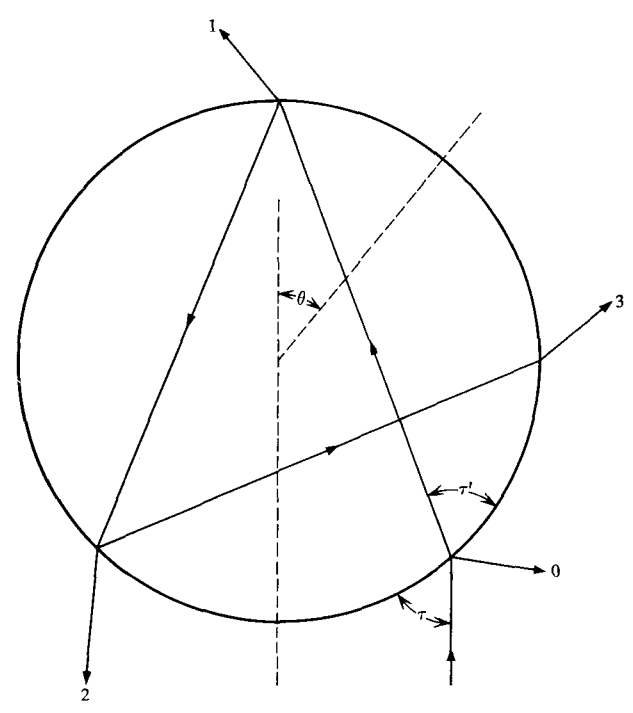


Figure 7 Path of a light ray through a sphere according to geometrical optics.

The rays entering the sphere at different angles but emerging in the same direction θ interfere and give rise to several maxima and minima in the intensity curve (supernumerary bows).^{3,28} For the primary rainbow, its supernumerary region ends at 167.3°. Similarly, after two internal reflections (p=3), we have a secondary rainbow at $\theta=126.8^\circ$ with its supernumerary region ending at 109.1°. The exact positions of the rainbows and its supernumerary maxima and minima for a sphere of given size can be obtained by following a procedure outlined by Van de Hulst.³

From the variations of I versus θ presented in Fig. 9 (curve A), it appears that there are several maxima and minima in the region of the secondary rainbow. However, from the results presented in a recent paper, ²⁸ it is clear that for a sphere of this size, ray optics predicts only two maxima, one at about 120° and the other at about 110°. Thus, one concludes that the presence of three maxima in the angular region 118°-132° is due to significant contributions from the radiations resulting from causes other than two internal reflections. This pseudorainbow feature is considerably suppressed when $n_2 = 5.0 \times 10^{-3}$ (curve B). For still higher absorption, there is no evidence of the feature. From Fig. 10, it can be seen that the rainbow region is strongly polarized.

The primary rainbow and its four supernumerary maxima can be clearly identified in the I vs θ values plotted in Fig. 11 for $n_2 = 1.0 \times 10^{-5}$. Furthermore, the

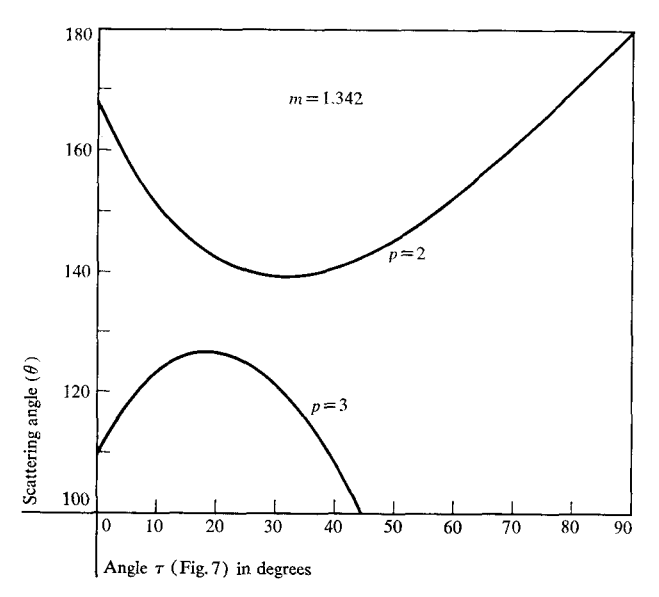
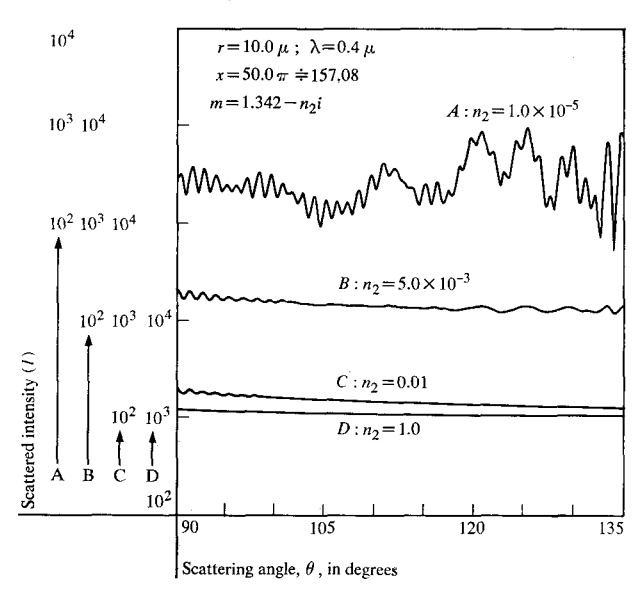


Figure 8 Scattering angle θ at which the ray emerges after suffering one (p=2) and two (p=3) internal reflections, versus the angle τ which the incident ray makes with the surface of the sphere.

Figure 9 Variation of the scattered intensity as a function of the scattering angle; $90^{\circ} \le \theta \le 135^{\circ}$.



region of the maxima shows very strong positive polarization (Fig. 12). For $n_2 = 5.0 \times 10^{-3}$, these features are much less suppressed than those of the secondary rainbow. Even the curve corresponding to $n_2 = 0.01$ shows some ripple. This is so because the rays giving rise to the primary rainbow travel shorter optical distances within the sphere than those giving rise to the secondary rainbow.

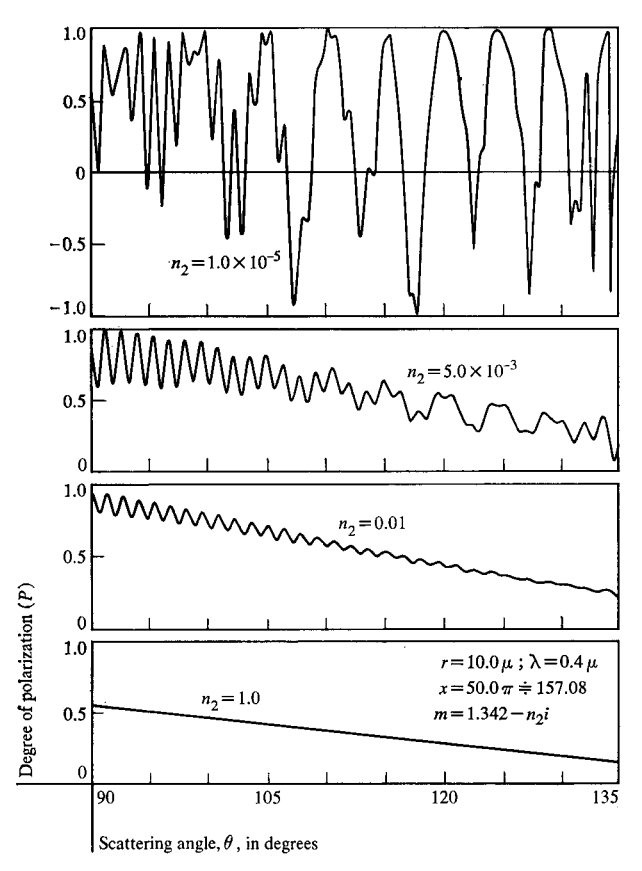


Figure 10 Variation of the degree of polarization of the scattered radiation as a function of the scattering angle; $90^{\circ} \leq \theta \leq 135^{\circ}$.

Another interesting feature of Fig. 11 is a general increase in the scattered intensity as θ is increased from 170° to 180°. There are several distinct maxima and minima which are strongly polarized (Fig. 12). This is the region of the glory. As mentioned earlier, the region of the primary rainbow ends at 167.3°. Hence, there is no obvious ray optics explanation for the phenomenon of glory. For a heuristic explanation, one is therefore forced to invoke the notion of surface waves on the sphere coupled with rays that jump through the sphere at the critical angle.3,23 However, the propagation of the waves on the spherical surface is only qualitatively understood. Since the remnants of glory can be seen even in the I vs θ and P vs θ curves for $n_2 = 0.01$, it may be possible to obtain a better understanding of the surface waves by analyzing the attenuation of the scattered radiation as a function of n_2 .

4. Concluding remarks

Even though Mie's expressions for evaluating the characteristics of the electromagnetic radiation scattered by a sphere were first derived in 1908, a numerical solution to the problem for a general case has run into several

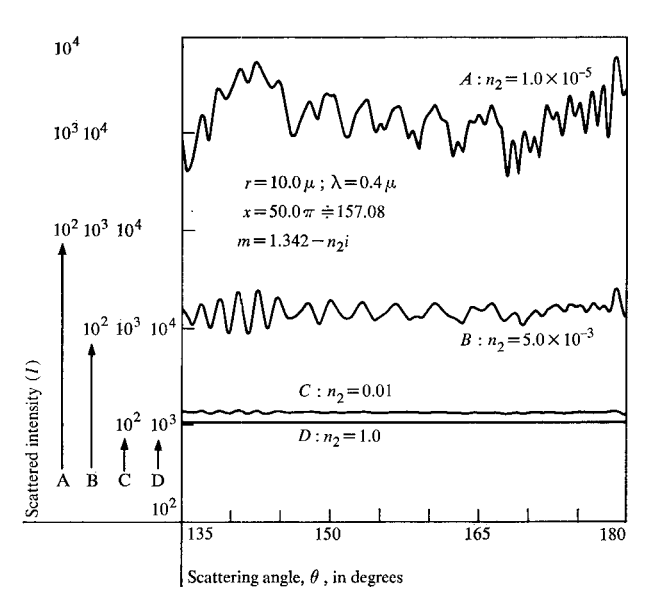
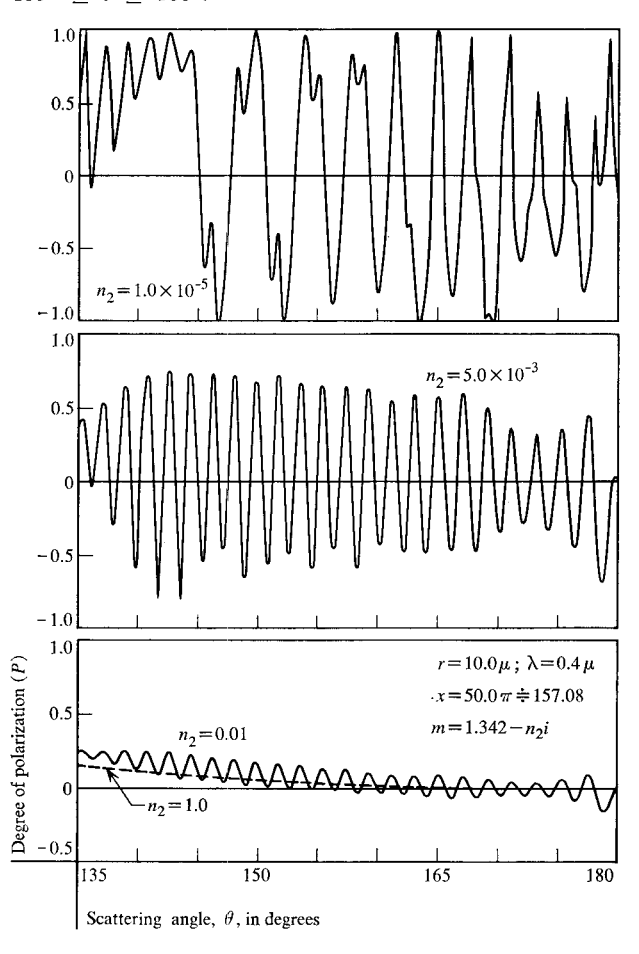


Figure 11 Variation of the scattered intensity as a function of the scattering angle; $135^{\circ} \le \theta \le 180^{\circ}$.

Figure 12 Variation of the degree of polarization of the scattered radiation as a function of the scattering angle; $135^{\circ} \leq \theta \leq 180^{\circ}$.



difficulties for a long time. After examining the problem in detail, a computer program in FORTRAN IV G language was recently developed.²⁷ Some of the highlights of this computer program along with sufficient numerical results are presented in the preceding sections to demonstrate the feasibility and reliability of such computations.

Acknowledgment

I wish to take this opportunity to express my sincere thanks to Dr. Baxter H. Armstrong for reading the first draft of this manuscript and for his valuable comments.

Appendix: Expressions for Mie Scattering

In order to describe the scattering process fully, it is necessary to represent a beam of radiation as a vector or as a one-column matrix (I) with four elements. In the Stokes representation, ²⁹ the first two elements of this matrix noted by I_c and I_r , represent the specific intensities of the beam in two directions e and r, respectively. The directions e and r are mutually at right angles to each other, such that the e-r plane is perpendicular to the direction of propagation of the radiation under study. The other two elements, viz., I_u and I_v , are needed for defining the direction of polarization with respect to the e-r plane, and the ellipticity of the beam respectively. Further details about the Stokes parameters and their relationships to the conventional radiation parameters can be found in several places.^{2,30}

The expressions for the radiation scattered by a sphere of radius r, and of material with a complex index of refraction m, have been aptly derived by Van de Hulst, and also by Born and Wolf. We shall therefore enumerate the final results only. Let \mathbf{I}_r and \mathbf{I}_s respectively represent the Stokes parameters of the radiation incident on, and scattered by, a sphere with e component parallel to the plane of scattering. Then

$$\mathbf{I}_{s} = \mathbf{F}' \cdot \mathbf{I}_{i}, \tag{25}$$

where F' is a four-by-four matrix referred to as a "transformation matrix" by Van de Hulst³⁶. It has the following form:

$$\mathbf{F}' = \begin{vmatrix} M_2 & 0 & 0 & 0 \\ 0 & M_1 & 0 & 0 \\ 0 & 0 & S_{21} & -D_{21} \\ 0 & 0 & D_{21} & S_{21} \end{vmatrix} . \tag{26}$$

The matrix F' and hence the matrix I_s are functions of the following parameters:

 $x = 2\pi r/\lambda$, where λ is the wavelength of the incident radiation:

 $m = n_1 - in_2$, index of refraction of the material of the sphere with respect to its surrounding;

and θ = the angle between the direction of the incident and that of the scattered radiation.

Van de Hulst³ has also noted that only three elements of **F**' are independent, the interrelationship being

$$S_{21}^2 + D_{21}^2 = M_2 M_1. (27)$$

In order to evaluate these elements, one first defines the complex amplitudes $S_1(x, m, \theta)$ and $S_2(x, m, \theta)$ for the scattered radiation.

$$S_1(x, m, \theta) \sum_{n=1}^{\infty} \frac{(2n+1)}{n(n+1)} \left[a_n(x, m) \pi_n(\mu) + b_n(x, m) \tau_n(\mu) \right]$$
 (28)

and

$$S_2(x, m, \theta) = \sum_{n=1}^{\infty} \frac{(2n+1)}{n(n+1)} \left[b_n(x, m) \pi_n(\mu) + a_n(x, m) \tau_n(\mu) \right], \tag{29}$$

where

$$\mu = \cos \theta. \tag{30}$$

Then,

$$M_{1} = S_{1}S_{1}^{*},$$

$$M_{2} = S_{2}S_{2}^{*},$$

$$S_{21} = \frac{1}{2}(S_{2}S_{1}^{*} + S_{1}S_{2}^{*}),$$

$$D_{21} = \frac{i}{2}(S_{2}S_{1}^{*} - S_{1}S_{2}^{*}).$$
(31)

The functions $a_n(x, m)$ and $b_n(x, m)$ are given by

$$a_n(x, m) = \frac{\Psi'_n(mx)\Psi_n(x) - m\Psi_n(mx)\Psi'_n(x)}{\Psi'_n(mx)\xi_n(x) - m\Psi_n(mx)\xi'_n(x)},$$
 (32)

and

$$b_n(x, m) = \frac{m\Psi'_n(mx)\Psi_n(x) - \Psi_n(mx)\Psi'_n(x)}{m\Psi'_n(mx)\xi_n(x) - \Psi_n(mx)\xi'_n(x)}$$
(33)

 $\Psi_n'(z)$ and $\xi_n'(x)$ are the derivatives of $\Psi_n(z)$ and $\xi_n(x)$ with respect to z and x, respectively.

$$\Psi_n(z) = z j_n(z) \tag{34}$$

$$\xi_n(x) = x[j_n(x) - iy_n(x)] \tag{35}$$

$$\Psi'_{n}(z) = z j_{n-1}(z) - n j_{n}(z)$$
 (36)

and

$$\xi'_n(x) = x[j_{n-1}(x) - iy_{n-1}(x)] - n[j_n(x) - iy_n(x)].$$
(37)

The functions j_n and y_n are the spherical Bessel functions of the first and second kind, respectively. The following recurrence relationships and initial values for setting up the recurrence procedure can be found in any of the standard mathematical books (e.g., Ref. 32).

$$f_{n+1}(z) = \frac{2n+1}{z} f_n(z) - f_{n-1}(z)$$

$$[f_n(z) : j_n(z), y_n(z)]. \tag{38}$$

$$j_{-1}(z) = -y_0(z) = \frac{\cos z}{z},$$
 (39)

and

$$j_0(z) = y_{-1}(z) = \frac{\sin z}{z}.$$
 (40)

J. V. DAVE

The phase functions $\pi_n(\mu)$ and $\tau_n(\mu)$ appearing in Eqs. (28) and (29) can be expressed in terms of the Legendre polynomials as

$$\pi_n(\mu) = \frac{dP_n(\mu)}{d\mu} \,, \tag{41}$$

$$\tau_n(\mu) = \mu \pi_n(\mu) - (1 - \mu^2) \frac{d\pi_n(\mu)}{d\mu}.$$
 (42)

Besides the elements of the transformation matrix F', other terms of considerable importance are the dimensionless constants referred to as "efficiency factors" by Van de Hulst, 37 Q_{ϵ} , the efficiency factor for extinction, which is the ratio of the total amount of energy removed from the incident beam to the geometric cross-section (πr^2) of the particle, can be obtained from the values of a_n and b_n only.

$$Q_{e}(x, m) = \frac{2^{\tau} \sum_{n=1}^{\tau} (2n+1) [\operatorname{Re}(a_{n}) + \operatorname{Re}(b_{n})]. (43)$$

The symbol Re stands for the real part of the quantity in parentheses. Q_s, the efficiency factor for scattering, is given by the following expression:

$$Q_{\bullet}(x, m) = \frac{2}{x^2} \sum_{n=1}^{\infty} (2n+1)[|a_n|^2 + |b_n|^2]$$
 (44)

If there is no absorption, i.e., $n_2 = 0$, $Q_e = Q_s$. Otherwise, Q_a , the efficiency factor for absorption, is given by

$$Q_a = Q_e - Q_s. (45)$$

Another dimensionless quantity of considerable interest is the so-called "asymmetry factor" represented by $\cos \theta$

$$\frac{1}{\cos \theta} = \frac{4}{x^2 Q_s} \sum_{n=1}^{\infty} \left\{ \frac{n(n+2)}{n+1} \operatorname{Re} \left(a_n a_{n+1}^* + b_n b_{n+1}^* \right) + \frac{2n+1}{n(n+1)} \operatorname{Re} \left(a_n b_n^* \right) \right\}$$
(46)

As noted by Irvine,10 and again by Kattawar and Plass12 [but not by Giese⁶], asterisks appearing in Eq. (46) have been omitted in Ref. 3.

The value Q_p , efficiency factor for radiation pressure, can then be obtained using the following:

$$Q_p = Q_e - \overline{\cos \theta} \cdot Q_s. \tag{47}$$

References

- 1. Lord Rayleigh, (J. W. Strutt), Phil. Mag. 41, 107-120 and 274-279 (1871).
- G. Mie, Ann. der Physik 25, 377-445 (1908).
- H. C. Van de Hulst, Light Scattering by Small Particles, John Wiley & Sons, Inc., New York, 470 pp. (1957).
- R. O. Gumprecht and C. M. Sliepcevich, Tables of Functions of First and Second Partial Derivatives of Legendre Polynomials, University of Michigan Press, Ann Arbor, Michigan, 310 pp. (1951).
- 5. R. O. Gumprecht and C. M. Sliepcevich, J. Phys. Chem. 57, 90-95 (1953).
- 6. R. H. Giese, Zeit. für Astrophysik 51, 119-147 (1961).
- 7. D. Deirmendjian, R. Clasen, and W. Viezee, J. Opt. Soc. Amer. 51, 620-633 (1961).
- 8. B. M. Herman, Quart. Journ. Roy. Met. Soc. 88, 143-150 (1962).
- 9. D. Deirmendjian and R. Clasen, Light Scattering on Partially Absorbing Homogeneous Spheres of Finite Size, R-393-PR, The Rand Corp., Santa Monica, Calif., 44 pp. (1962).

- 10. W. M. Irvine, Bull. Astron. Inst. Neth. 17, 176-184 (1963)
- 11. W. M. Irvine, Jour. Opt. Soc. Amer. 55, 16-21 (1965). 12. G. W. Kattawar and G. N. Plass, Applied Optics 6,
 - 1377-1382 and 1549-1554 (1967)
- 13. K. Cunningham, M. B. Wells, and D. G. Collins, "Light Transport in the Atmosphere, Vol. II: Machine Codes for Calculation of Aerosol Scattering and Absorption Coefficients", Radiation Research Assoc., Inc., Fort Worth, Texas, Technical Report No. ECOM-00240-1, 128 pp. (1966).
- 14. G. N. Plass, Applied Optics 5, 279-285 (1966); [Also refer to letter to editor, 7, 985-986 (1968)1.
- 15. W. M. Irvine and J. B. Pollack, Icarus 8, 324-360 (1968)
- 16. R. H. Giese, E. DeBary, K. Bullrich, and C. D. Vinnemann, Tabellen Der Streufunktionen i_1 (φ), i_2 (φ) und des Streuquerschnittes K(a, m) Homogener Kugelchen nach der Mie'schen Theorie, Abhandlungen der Deutschen Akademie der Wissenschaften zu Berlin, Akademie-Verlag-Berlin, 175 pp. (1962)
- 17. R. Hickling, J. Opt. Soc. Amer. 58, 455-460 (1968).
- 18. H. H. Denman, W. J. Pangonis and W. Heller, Angular Scattering Functions for Spheres, Wayne State University Press, Detroit, Michigan, 294 pp. (1966).
- 19. R. S. Fraser, Scattering Properties of Atmospheric Aerosols, Scientific Report No. 2, Contract No. AF 19(604)-2429, Department of Meterology, University of California at Los Angeles, 183 p. (Oct. 1959).
- 20. D. Deirmendjian, Applied Optics, 3, 187-196 (1964)
- 21. E. DeBary, B. Braun and K. Bullrich, Tables Related to Light Scattering in a Turbid Atmosphere, Vol. I, II, and III, AFCRL-65-710 (I) to 710 (III), Special Report No. 33, Optical Physics Laboratory Project 7621, Air Force Cambridge Research Laboratories, Bedford, Mass., 859 pp. (Sept. 1965)
- 22. R. Eiden, Applied Optics, 5, 569-575 (1966).
- T. S. Fahlen and H. C. Bryant, J. Opt. Soc. Amer. 58, 304-310 (1968).
- 24. M. Abramowitz, Handbook of Mathematical Functions, edited by M. Abramowitz and I. A. Stegun, National Bureau of Standards, Applied Mathematics Series: 55, pp. IX-XIV (1964).
- 25. J. C. P. Miller, Proc. Cambridge Phil. Soc., 48, 428-435
- 26. F. J. Corbató and J. L. Uretsky, J. Assoc. Computing Machinery, 6, pp. 366-375 (1959).
- 27. J. V. Dave, Subroutines for Computing the Parameters of the Electromagnetic Radiation Scattered by a Sphere, Report No. 320-3237, IBM Scientific Center, Palo Alto. California, 65 pp. (May 1968).
- 28. J. V. Dave, Applied Optics, 8, 155-164 (1969)
- 29. G. C. Stokes, Trans. Camb. Phil. Soc. 9, 399 (1852).
- 30. S. Chandrasekhar, Radiative Transfer, Clarendon Press, Oxford, England, 393 pp. (1950).
 31. M. Born and E. Wolf, *Principles of Optics*, Pergamon
- Press, New York, 808 pp. (1959).
- 32. H. A. Antosiewicz, Handbook of Mathematical Functions, edited by M. Abramowitz and I. A. Stegun, National Bureau of Standards, Applied Mathematics Series: **55**, pp. 435–478 (1964).
- L. Infeld, Quart. J. Applied Math. 5, 113-132 (1947).
 A. L. Aden, J. Applied Physics, 22, 601-605 (1951).
- 35. U. S. National Bureau of Standards, Tables of n! and $\Gamma(n + 1/2)$ for the first thousand values of n, Applied Mathematics Series: 16, U. S. Government Printing Office, Washington, D. C. (1951).
- 36. Van de Hulst, op. cit., p. 44.
- 37. Van de Hulst, op. cit., pp. 14 and 127.

Received August 8, 1968